Abrupt tectonics and rapid slab detachment with grain damage

David Bercovici[a,1], Gerald Schubert[b], and Yanick Ricard[c]

[a]Department of Geology & Geophysics, Yale University, New Haven, CT 06520; [b]Department of Earth, Planetary & Space Sciences, University of California, Los Angeles, CA 90095; and [c]Laboratoire de Géologie de Lyon, Ecole Normale Supérieure de Lyon, Université de Lyon-1, CNRS, 69364 Lyon Cedex 07, France

Edited by Peter L. Olson, Johns Hopkins University, Baltimore, MD, and approved December 17, 2014 (received for review August 11, 2014)

A simple model for necking and detachment of subducting slabs is developed to include the coupling between grain-sensitive rheology and grain-size evolution with damage. Necking is triggered by thickened buoyant crust entrained into a subduction zone, in which case grain damage accelerates necking and allows for relatively rapid slab detachment, i.e., within 1 My, depending on the size of the crustal plug. Thick continental crustal plugs can cause rapid necking while smaller plugs characteristic of ocean plateaux cause slower necking; oceanic lithosphere with normal or slightly thickened crust subducts without necking. The model potentially explains how large plateaux or continental crust drawn into subduction zones can cause slab loss and rapid changes in plate motion and/or induce abrupt continental rebound.

subduction zones | slab detachment | plate tectonics | continent rebound

Subduction of tectonic plates is widely recognized as the manifestation of a convecting mantle, i.e., where the cold convective thermal boundary layer at the Earth's surface becomes heavy enough to sink (e.g., refs. 1 and 2). Subduction is similarly recognized for being the primary driving force for tectonic motions (3, 4) as well as controlling vertical displacements of continents in convergent margins (5, 6). Subducting slabs, however, can become detached from their originating plate, possibly by either a necking instability or by plastic or brittle failure (see refs. 7 and 8). Such detachment has been invoked to explain seismicity gaps and pinched tomographic features in slab structures (9, 10). However, slab detachment also has significant geodynamic consequences and may help account for precipitous tectonic events that are not readily explained by mantle convective motions (11). In particular, rapid loss of a slab from its connected plate could cause a sudden change in plate forces and hence abrupt change in plate motion. Likewise, slab loss below continents could account for instances of rapid uplift. In both cases, horizontal or vertical adjustments occur on the order of a few million years, which is much more rapid than the typical 10- to 100-My timescale for changes in convective circulation (i.e., typical transit times across the mantle).

The trigger for slab loss must also be reasonably rapid and induce a change in the subducting system that causes it to neck or break off rather than continue subducting. One plausible trigger is the arrival of thick buoyant crust swept into the subduction zone, which would likely have little influence until its actual arrival; this would potentially impede subduction and introduce tensile stresses that could initiate detachment. This process could, for example, be associated with the arrival of thick oceanic plateaux (or midocean ridges) at subduction zones and subsequent changes in plate motion. For example, the collision of the Ontong Java Plateau with the Melanesian arc possibly curtailed subduction and caused a rotation of the Pacific plate at 6 Ma (12). Although highly speculative, ingestion of a plateau into the Aleutian trench at 50 Ma may have abruptly disrupted plate forces, causing the sudden change in plate motion associated with the Emperor-Hawaiian bend. Moreover, when thick continental crust is entrained into a subduction zone, the slab can also detach (13), and this is possibly associated with a rapid isostatic uplift of the overriding plate. This process is apparent in the correlation between the tectonic evolution of various margins with tomographic images of slabs (e.g., ref. 9). Slab detachment has thus been invoked to explain the topographic and tectonic changes at Vanuatu (14), the Alps and the Aegean (13), the Dabie shan (15), the Pannonian Basin (16), Central America (10), Borneo (17), Anatolia (18, 19), Taiwan (20), East Timor (21), the Appenines (22), and during the Messinian Event (23, 24).

The first numerical models of slab detachment, based on diffusion and dislocation creep rheologies for olivine, found that the slab was too cold and stiff to detach in the short timescale implied by geological observations (25). More recent studies, however (7, 8), were able to obtain more rapid detachment, but required a power-law behavior in excess of normal dislocation creep, and/or a combination of multiple lithologic layers with various self-weakening effects (non-Newtonian behavior, shear heating, brittle failure, and sediment ingestion).

We propose a simple model for rapid slab detachment that combines triggering by entrainment of buoyant crust, and a rapid necking mechanism facilitated by the coupling of grain-sensitive rheology and grain-size evolution with damage (26–31). In particular, grain reduction and weakening by the combination of damage and Zener pinning in a multiphase mineralogical assemblage, which is consistent with field and laboratory observations of polycrystalline rocks (27), allows rapid necking and thus abrupt detachment. The stress drop in the slab during detachment also provides an estimate for how quickly the slab decouples from the surface and changes plate forces and/or loading for continental subsidence. With a sufficiently large buoyant crustal plug and substantial damage, rapid necking occurs on the order of 1 My; this suggests that the introduction of large ocean plateaux or continental crust into convergent margins can trigger precipitous detachment, and thus abrupt horizontal or vertical changes in tectonic motion.

Significance

Subduction zones are delineated by Earth's ocean trenches, and are where tectonic plates sink into the mantle as cold heavy slabs, which in turn drive plate motion. But slabs can detach from their surface plates, thus altering tectonic driving forces. Slab detachment can occur if thick crust from continents or oceanic plateaux is swept by plate motion into the subduction zone, thus plugging it up. Detachment is also accelerated because mineral grains in the slab become smaller during deformation, causing the slab to weaken rapidly while being stretched. The combination of crustal plugs with weakening causes abrupt slab detachment in a few million years, which can account for observed precipitous changes in plate tectonic motion and rapid continental uplift.

Author contributions: D.B., G.S., and Y.R. designed research; D.B. performed research; and D.B. wrote the paper.

The authors declare no conflict of interest.

This article is a PNAS Direct Submission.

[1]To whom correspondence should be addressed. Email: david.bercovici@yale.edu.

A Simple Necking Model

Force Balance and Stress. We consider a subducting slab of original thickness D_0 and length $H_0 > D_0$, which undergoes necking after thickened buoyant crust plugs up the subduction zone, thereby causing excess tensile stress along the slab. In the absence of this crustal plug, e.g., before its arrival at the subduction zone, tensile stress in the slab is assumed small enough that the slab does not deform, in which case its effective weight is supported by mantle viscous drag and it readily pulls the trailing plate into the subduction zone. With this assumption, necking of the slab cannot occur without a plug. However, with the ingestion of the crustal plug, the upper portion of the slab necks and has length $h(t)$ and width $b(t)$ after some time t (Fig. 1). Although here we isolate the effect of the crustal plug on slab necking, it can also induce other responses such as slab flattening or trench retreat (e.g., refs. 32–34).

In general, the negative buoyancy of the slab causes a downward force F_S (units of Newtons per meter for this 2D model), the positive buoyancy of the thick crustal plug causes an upward force F_C, and mantle drag on the descending slab causes an upward force F_D on either side of the slab. We first define a basic state where, before necking occurs, the full negative buoyancy of the slab is F_S° and the full mantle drag is F_D° and all these forces balance

$$F_C - F_S^\circ + 2F_D^\circ = 0 \qquad [1]$$

where $F_S^\circ = \Delta\rho g D_0 H_0$, $F_D^\circ = \mu_0 H_0 W_0 / L$ wherein $\Delta\rho$ is the effective net slab density anomaly (accounting for thermal and chemical density variations and the effect of phase changes, assuming they sum to yield a net negative buoyancy and slab driving force), μ_0 is the surrounding mantle viscosity, and W_0 is the slab descent speed; L is the horizontal distance over which shear occurs, and is assumed to be a characteristic plate length or convection cell width that is roughly the same as the mantle depth (i.e., $L \approx 3000$ km). (See Table 1 for fixed material and model properties.) With this basic force balance, the slab still descends, but more slowly than if the continental plug were not present (i.e., if $F_C = 0$).

When necking and stretching ensues, we assume there is a necking portion of initial length h_0, and the rest of the slab of length $H_0 - h_0$ remains undeformed. The necking portion initiates near the top of the slab where the tensile stress is maximum, and assuming the self-weakening feedback caused by necking and damage induces much larger strength heterogeneity

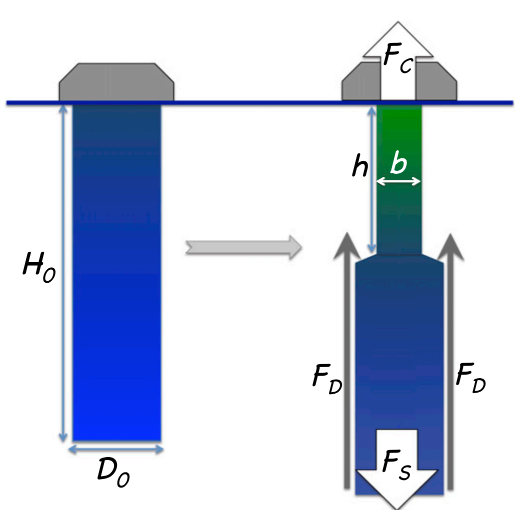

Fig. 1. Sketch of model configuration, with basic initial geometry on the left and the necking geometry and forces on the right. See *A Simple Necking Model, Force Balance and Stress*, for discussion.

Table 1. Fixed material and model properties

Quantity	Symbol	Value
Crustal density	ρ_c	2,700 kg/m^3
Mantle–crust density contrast	$\Delta\rho_c$	600 kg/m^3
Gravitational acceleration	g	10 m/s^2
Mean mantle viscosity	μ_0	10^{22} Pa s
Initial slab width	D_0	100 km
Initial slab length	H_0	1,500 km
Plate length (mantle depth)	L	3,000 km
Dislocation creep exponent	n	3
Dislocation creep compliance	A	2×10^{-41} s$^{-1}\cdot$Pa^{-n}
Diffusion creep grain size exponent	m	3
Diffusion creep compliance	B	5×10^{-37} s$^{-1}\cdot$Pa$^{-1}\cdot$m^m
Interface coarsening rate	G	2×10^{-38} m$^q\cdot$s^{-1}
Interface coarsening exponent	q	4
Interface surface tension	γ	1 Pa m

in the slab than might occur at greater depth by, for example, solid–solid phase changes (35, 36). The viscous vertical tensile stress τ in the necking portion pulls up on the top of the undeformed slab, in which case the force balance on that undeformed portion is

$$\tau \cdot b - F_S + 2F_D = 0 \qquad [2]$$

where b is the time-dependent width of the slab where it necks, $F_S = \Delta\rho g D_0 (H_0 - h_0)$, $F_D = \mu_0 (H_0 - h_0)(W_0 + w)/L$, and w is the additional slab descent velocity because of necking. Using Eq. **1** to eliminate W_0 from Eq. **2**, we obtain

$$\tau = \frac{1}{b}\left(\frac{H_0 - h_0}{H_0}\right)\left(F_C - \frac{2\mu_0 H_0 w}{L}\right) = \frac{1}{b}(F_C' - 2\mu_0' w) \qquad [3]$$

which thus defines the reduced plug force F_C' and reduced mantle viscosity μ_0'. The tensile stress τ depends on the crustal buoyancy pulling up as well as the fractional length of heavy undeformed slab pulling down; in the simple limit where there is no continental plug and no necking, $\tau = 0$ and the slab subducts without stretching. Likewise, in the similar analytical model of ref. 7, there is no mantle drag, and the slab is supported by a rigid top surface, in which case, by Newton's third law (37), $F_C = F_S^\circ$.

Although the necking portion starts with length $h = h_0$ and width $b = D_0$, it becomes narrower and longer. We assume the mass of the necking region is conserved; hence hb is a constant. Moreover, we assume $h_0 = \alpha D_0$, which is half the wavelength of the initial infinitesimal necking instability (38, 39); α itself is dependent on rheology, and for our model, with a Newtonian surrounding mantle and a slab initially in dislocation creep (see *Rheology*), $\alpha \approx 5$. Therefore, $hb = \alpha D_0^2$, and since $w = dh/dt$, then

$$w = -\frac{\alpha D_0^2}{b^2}\frac{\mathrm{d}b}{\mathrm{d}t} \qquad [4]$$

The stress relation (Eq. **3**) thus becomes

$$\tau = \frac{F_C'}{b} + 2\mu_0' \frac{\alpha D_0^2}{b^3}\frac{\mathrm{d}b}{\mathrm{d}t} \qquad [5]$$

Note that this simple necking model makes several key assumptions, namely that the stretching of the slab is initially nearly uniform before the necking instability starts (38) (which is valid provided H_0 is appreciably longer than h_0) and that the necking portion of length $h(t)$ remains approximately uniform in width $b(t)$.

Rheology. The strain rate of necking is related to the stress by a composite rheology of dislocation and diffusion creep in a polycrystalline rock, i.e., predominantly peridotite:

$$\dot{e}=\frac{w}{h}=-\frac{1}{b}\frac{\mathrm{d}b}{\mathrm{d}t}=A\tau^n+B\frac{\tau}{r^m} \quad [6]$$

where A and B are the effective dislocation and diffusion creep compliances for a mixture of olivine and pyroxene (which we assume, for simplicity, to have similar rheological properties), and we use the exponents $n=m=3$ for standard dislocation and Coble creep. Although diffusion creep depends on the evolving grain size, the interface between the rock's mineral phases (i.e., olivine and pyroxene) induces Zener pinning, which blocks grain growth (40–42). Thus, we assume grain size evolution is slaved to the evolution of the size of the pinning bodies r, which is equivalent to the characteristic radius of curvature, or roughness of the interface (27–29). Hence, the mineral grain size is proportional to r, and using the definition for a pinned-state (27), the rock's average grain size is approximately $\frac{\pi}{2}r$. (The pinned state requires that the Zener pinning factor $\mathcal{Z}_i=1-\mathfrak{c}(1-\phi_i)(R_i/r)^2=0$, where R_i is grain size of phase i with volume fraction ϕ_i, and $\mathfrak{c}=0.87$ for the grain size distributions used by refs. 27–29. The mean grain size is thus $\overline{R}=\sum_i\phi_iR_i=\sum_i r\phi_i/\sqrt{\mathfrak{c}(1-\phi_i)}$, and for a peridotitic mixture with $\phi_1=0.4$ for pyroxene and $\phi_2=0.6$ for olivine, this leads to $\overline{R}=1.5707r\approx\frac{\pi}{2}r$.)

Grain Evolution, Pinning, and Damage. The evolution equation for the pinning body size (or interface roughness) r, which controls grain size, is

$$\frac{\mathrm{d}r}{\mathrm{d}t}=\frac{\eta G}{qr^{q-1}}-\frac{fr^2}{\gamma\eta}\Psi \quad [7]$$

where most parameters are defined in Table 1, save for f, which is a damage partitioning fraction (determining how much deformational work goes to creating surface energy to make smaller pinning bodies and hence smaller grains), and $\eta=3\phi_1\phi_2$. Although $f\ll 1$ (a typical value at midlithosphere temperature is 10^{-4}; see ref. 31), we consider a range of values through variation of the dimensionless damage number (see *Dimensionless Governing Equations*). Finally, $\Psi=\tau\dot{e}=A\tau^{n+1}+B\tau^2/r^m$ is the deformational work. (See refs. 27–29, for more details and applications of the grain damage and pinning theory.)

Dimensionless Governing Equations. The governing equations for our system are Eqs. **5–7**, which we nondimensionalize using D_0 as the length scale for b, F_c'/D_0 as the scale for τ, and time and pinning body (or grain) size scales for t and r given by

$$\mathrm{T}=\frac{1}{A}\left(\frac{D_0}{F_c'}\right)^n \quad \text{and} \quad \mathrm{R}=\left[\frac{B}{A}\left(\frac{D_0}{F_c'}\right)^{n-1}\right]^{1/m}, \quad [8]$$

respectively. The timescale T is the inverse strain rate for slab necking by dislocation creep, which is how the slab initially deforms; the relation for the grain/pinning body scale R is the field boundary between diffusion and dislocation creep (i.e., when their strain rates are equal). The dimensionless governing equations are thus

$$\tau=\frac{1}{b}+\frac{\beta}{b^3}\frac{\mathrm{d}b}{\mathrm{d}t} \quad [9]$$

$$\frac{\mathrm{d}b}{\mathrm{d}t}=-b\left(\tau^n+\frac{\tau}{r^m}\right) \quad [10]$$

$$\frac{\mathrm{d}r}{\mathrm{d}t}=\frac{\mathcal{C}}{qr^{q-1}}-\mathcal{D}r^2\left(\tau^{n+1}+\frac{\tau^2}{r^m}\right) \quad [11]$$

The dimensionless parameters of the model are $\alpha=h_0/D_0$ as described above, and

$$\beta=2\mu_0'\alpha A\left(\frac{F_c'}{D_0}\right)^{n-1}, \mathcal{C}=\frac{\eta G\mathrm{T}}{\mathrm{R}^q} \quad \text{and} \quad \mathcal{D}=\frac{f\mathrm{R}}{\gamma\eta}\frac{F_c'}{D_0} \quad [12]$$

which are an effective viscosity ratio between the mantle and initially deforming slab, the coarsening (or healing) number, and damage number, respectively.

The dimensionless numbers are obtained using the rheological and grain growth and pinning-surface coarsening parameters from refs. 27–29 and 31 for midlithosphere at temperature $T\approx 1{,}000$ K (however, see ref. 29, Methods, for discussion of coarsening rate activation energy), which lead to the compliances and coarsening rates shown in Table 1, among other fixed parameters. For the crustal buoyancy stress, we use $F_c/D_0=\Delta\rho_c g\mathrm{h}_c$ where h_c is the effective crustal thickness, which we vary to assess the effect of different sized crustal plugs. The variation of h_c basically only affects the dimensionless number β. The coarsening number is always very small, and we conservatively fix it to $\mathcal{C}\approx 10^{-5}$; however, given the variations in the partitioning fraction f, we consider a range of damage numbers, given by $0\le\mathcal{D}\le 1{,}000$. Finally, as already noted earlier, we fix $\alpha=5$.

Necking Results

Simple Case of Steady-State Damage/Healing and All Diffusion Creep. We first consider the simple limiting case proposed by Schmalholz (7) in which there is no mantle drag supporting the slab, which simply hangs from a rigid lithosphere. We further consider that the slab has reached a steady state in which $dr/dt\to 0$ so that healing and damage are in balance; in this limit, the grains have been reduced so the rheology is dominated by diffusion creep. With these assumptions, the evolution Eqs. **10** and **11** become

$$\frac{\mathrm{d}b}{\mathrm{d}t}=-\frac{b\tau}{r^m} \quad [13]$$

$$\frac{\mathcal{C}}{qr^{q-1}}=\mathcal{D}\frac{\tau^2}{r^{m-2}} \quad [14]$$

which, when combined to eliminate r, yield

$$\frac{\mathrm{d}b}{\mathrm{d}t}=-b\tau\left(\frac{q\mathcal{D}\tau^2}{\mathcal{C}}\right)^{\frac{m}{q+1-m}}=-b\tau^4\left(\frac{q\mathcal{D}}{\mathcal{C}}\right)^{3/2} \quad [15]$$

using m and q from Table 1; this relation for $\dot{b}$ is equivalent to the Schmalholz relation with a stress power law exponent of $\mathfrak{n}=4$. Thus, the damage relation potentially gives an even stronger power-law necking effect than simple dislocation creep with $\mathfrak{n}=n=3$ (i.e., any $\mathfrak{n}>1$ leads to the necking instability, and the time to completely neck or break off the slab in the Schmalholz analysis is $t\approx 1/\mathfrak{n}$). Moreover, ref. 8. found that the best fit of the Schmalholz relation to their numerical experiments, which included a combination of various weakening effects, was also for $\mathfrak{n}=4$. For grain-damage weakening, the coefficient multiplying $-b\tau^4$ on the right side of Eq. **15** is very large, i.e., $(q\mathcal{D}/\mathcal{C})^{3/2}\approx 10^{10}$, using $q=4$, $\mathcal{C}=10^{-5}$ and $\mathcal{D}=10$, and this factor influences the necking rate. However, unlike Schmalholz's analysis, b does not collapse to 0 in a finite time, primarily because of the inclusion of mantle drag in our model.

Nonlinear Evolution and Necking. The full nonlinear governing Eqs. **9–11** can be solved numerically by first combining Eqs. **9** and **10** into a polynomial (cubic if $n=3$) for τ, the real solutions of which give the function $\tau(b,r)$; this is then used in Eqs. **10** and **11**, which are integrated using a stiff ordinary differential equation solver in MATLAB. The initial conditions are $b=1$ (100-km-thick slab) and $r=10$ (which corresponds to about 1-mm grain or pinning body size).

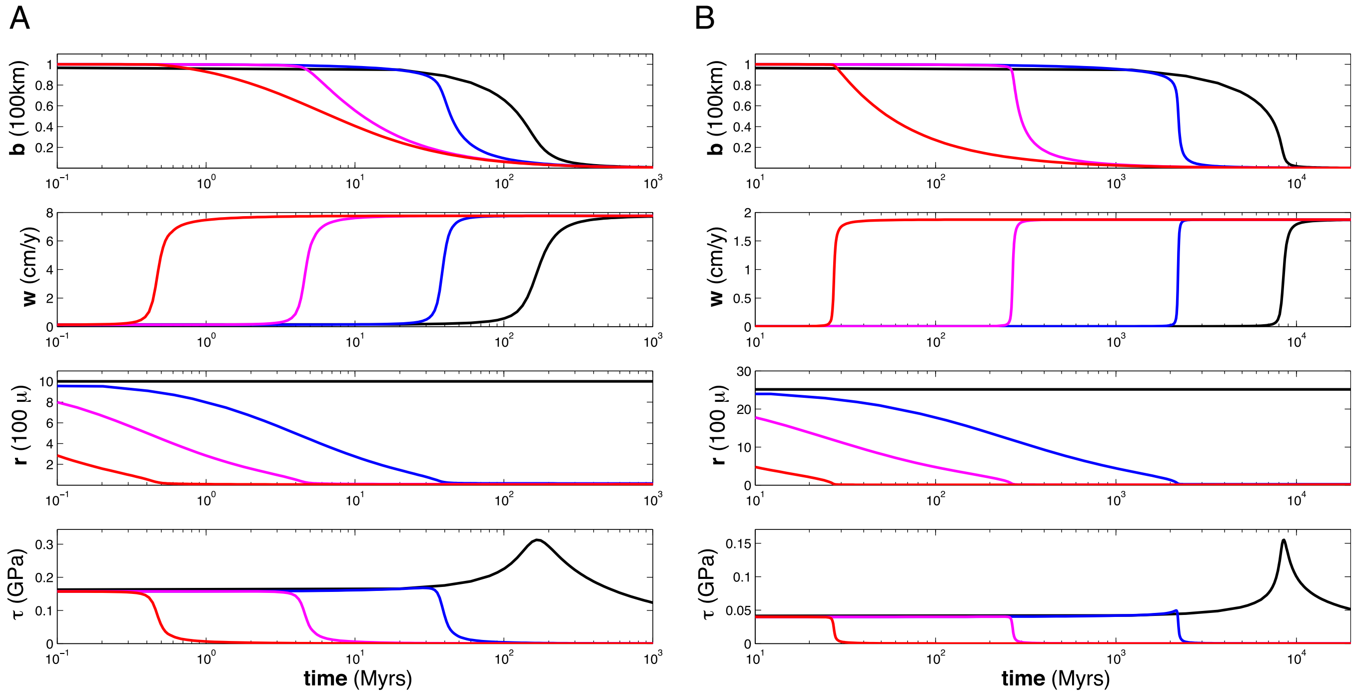

Fig. 2. Nonlinear solutions to Eqs. **9**–**11** for two cases of a 40-km-thick crustal plug with $\beta = 1.7 \times 10^{-2}$ (*A*) and a 10-km-thick crustal plug with $\beta = 1.1 \times 10^{-3}$ (*B*). Other parameters are $\mathcal{C} = 10^{-5}$, $\alpha = 5$, and four values of the damage number $\mathcal{D} = 0$, 10, 100, 1,000 in black, blue, magenta, and red, respectively. Initial conditions for dimensionless quantities are $b = 1$ and $r = 10$.

In this model, necking is triggered by a buoyant plug that imposes a tensile stress on the slab, which slows it down and causes it to neck. For the largest plug considered, with an equivalent $\mathbf{h}_c$ = 40-km-thick crust, the necking time is very long, of order 100 My, without any damage, but is reduced to about 1 My with significant grain damage (see Fig. 2*A*). However, for a much smaller continental plug (with a 10-km-thick crust), the necking time for each case goes up by almost two orders of magnitude; this is to be expected, since the timescale given by Eq. **8** goes as h_c^{-n} and thus a factor of 4 drop in h_c, with a power-law index $n = 3$, gives a factor of 64 increase in the basic timescale.

During necking, the slab width eventually drops to a finite value of several tens of meters but does not reach zero thickness. However, in principle, the slab neck cannot stretch longer than the depth of the mantle (minus the length of the undeformed slab). The maximum neck length is $h_{\max} = L - H_0 + h_0 \approx 2{,}000$ km (see Table 1), and this is associated with a neck width $b = \alpha D_0^2 / h_{\max} \approx 25$ km. However, the neck reaches this width (Fig. 2) at a considerably later time than the time for stress loss, and thus the full effect of detachment is "felt" well before the slab reaches the bottom of the mantle.

The additional velocity of slab descent w due to necking increases to values of 1–10 cm/y, which restores the total slab velocity to its free Stokes descent (i.e., the slab goes from a slower velocity, given the resistance of the buoyant crustal plug, to a faster velocity of a free-falling detached slab).

The stress τ of the neck on the descending slab (and hence the stress of the slab on the surface) increases and peaks over a long time when there is no damage, but drops precipitously, within about 1 My, when there is significant damage and a large crustal plug. This implies the stress guide or direct coupling of the slab to the surface is rapidly lost, which would induce a rapid loss of plate driving force and hence a change in plate motion, and/or a rapid uplift of overlying continent. The effect of detachment is most pertinent with regard to stress loss, and thus we infer the detachment time as the time needed to lose most of the stress τ; as expected, this detachment time is a strong function of crustal plug thickness h_c and damage number $\mathcal{D}$ (Fig. 3). For large plug size (30–40 km) and damage ($\mathcal{D} > 100$), the detachment time is of order 1 M. However, once the plug thickness h_c is less than 10–20 km, detachment takes 10–100 My or more (unless damage is extremely high).

Discussion and Conclusion

Our simple model demonstrates that the introduction of a significant buoyant crustal plug into a subduction zone can induce

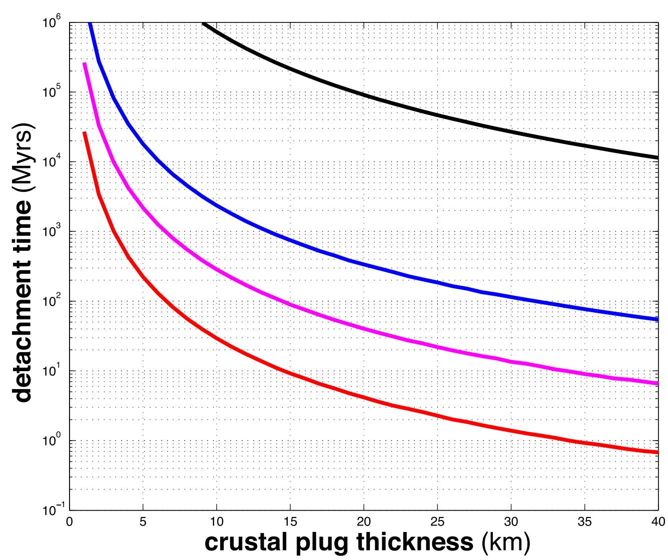

Fig. 3. Detachment time (defined as the time for stress τ to reach 10% of its maximum value) as a function of crustal plug thickness h_c, for damage numbers $\mathcal{D} = 0$, 10, 100, 1,000 in black, blue, magenta, and red, respectively. All other parameters are the same as in Fig. 2.

rapid slab detachment, provided there is a sufficient self-weakening mechanism in the slab. The weakening mechanism in our model is based on grain reduction and damage in polycrystalline rocks that is consistent with laboratory and field observations of mylonitic shear localization (27). With significant and plausible damage, detachment can occur in about 1 My for larger crustal plugs. However, as the crustal plug thickness is reduced, the detachment time increases rapidly, and for plugs much less than 10–20 km thick, detachment is typically 10–100 My or more (depending on the extent of damage), which is too slow to occur before convective downwelling of the slab sweeps away its necking portion into the lower mantle.

For the fastest model detachments, the stress drop is abrupt and would potentially induce a precipitous adjustment in forces driving horizontal plate motion, and/or vertical uplift/downwarping of continents in convergent margins. The stress drop in the model is effectively always simply $F_C'/D_0 = F_C/D_0 \cdot (H_0 - h_0)/H_0$. For the parameters used (Table 1), the stress drop is approximately 2/3 the total stress due to the crustal load F_C: In essence, only the bottom portion of the slab detaches, but the remaining necking portion still provides a vertical load even as it is being stretched. Thus, if, for example, a maximum 40 km of a crustal plug was submerged, after detachment, only 27 km of it would be restored to isostasy. However, the release of 27 km of crustal load to isostasy would lead to a significant 27 km $\cdot \Delta\rho_c/(\rho_c + \Delta\rho_c) = 5$ km surface uplift.

The stress loss associated with detachment is also equivalent to losing $(H_0 - h_0)/H_0 \approx 2/3$ of the slab driving force. This drop in driving force is sufficient to make a fast-moving plate approach speeds of a slow-moving plate, and/or allow the slab driving force elsewhere on the plate edge (that is not detached) to dominate and change plate directions. If detachment is in 1 My, as implied for the cases with large crustal loads and substantive damage, then this change in plate motion would appear as abrupt as what is observed for rapid changes in plate direction.

ACKNOWLEDGMENTS. The authors are grateful for thoughtful comments from the editor and two anonymous reviewers. This work was supported by National Science Foundation Grant EAR-1344538.

1. Schubert G, Turcotte D, Olson P (2001) *Mantle Convection in the Earth and Planets* (Cambridge Univ Press, New York).
2. Bercovici D (2003) The generation of plate tectonics from mantle convection. *Earth Planet Sci Lett* 205:107–121.
3. Forsyth D, Uyeda S (1975) On the relative importance of the driving forces of plate motion. *Geophys J R Astron Soc* 43:163–200.
4. Vigny C, Ricard Y, Froidevaux C (1991) The driving mechanism of plate tectonics. *Tectonophysics* 187:345–360.
5. Gurnis M (1990) Bounds on global dynamic topography from phanerozoic flooding of continental platforms. *Nature* 344:754–756.
6. Gurnis M (1993) Phanerozoic marine inundation of continents driven by dynamic topography above subducting slabs. *Nature* 364:589–593.
7. Schmalholz SM (2011) A simple analytical solution for slab detachment. *Earth Planet Sci Lett* 304:45–54.
8. Duretz T, Schmalholz SM, Gerya TV (2012) Dynamics of slab detachment. *Geochem Geophys Geosyst* 13:Q03020.
9. Wortel MJ, Spakman W (2000) Subduction and slab detachment in the Mediterranean-Carpathian region. *Science* 290(5498):1910–1917.
10. Rogers R, Karason H, van der Hilst R (2002) Epeirogenic uplift above a detached slab in northern Central America. *Geology* 30:1031–1034.
11. Richards M, Lithgow-Bertelloni C (1996) Plate motion changes, the Hawaiian-Emperor bend, and the apparent success and failure of geodynamical models. *Earth Planet Sci Lett* 137:19–27.
12. Austermann J, et al. (2011) Quantifying the forces needed for the rapid change of Pacific plate motion at 6Ma. *Earth Planet Sci Lett* 307:289–297.
13. von Blanckenburg F, Davies J (1995) Slab breakoff—A model for syncollisional magmatism and tectonics in the Alps. *Tectonics* 14:120–131.
14. Chatelain J, Molnar P, Prevot R, Isack B (1992) Detachment of part of the downgoing slab and uplift of the New Hebrides (Vanuatu) Islands. *Geophys Res Lett* 19:1507–1510.
15. Davies J, von Blanckenburg F (1995) Slab breakoff—A model of lithosphere detachment and its test in the magmatism and deformation of collisional orogens. *Earth Planet Sci Lett* 129:85–102.
16. Nemcok M, Pospisil L, Lexa J, Donelick R (1998) Tertiary subduction and slab break-off model of the Carpathian-Pannonian region. *Tectonophysics* 295:307–340.
17. Morley CK, Back S (2008) Estimating hinterland exhumation from late orogenic basin volume, NW Borneo. *J Geol Soc London* 165:353–366.
18. Faccenna C, Bellier O, Martinod J, Piromallo C, Regard V (2006) Slab detachment beneath eastern Anatolia: A possible cause for the formation of the North Anatolian fault. *Earth Planet Sci Lett* 242(1-2):85–97.
19. Schildgen TF, et al. (2012) Multi-phased uplift of the southern margin of the Central Anatolian plateau, Turkey: A record of tectonic and upper mantle processes. *Earth Planet Sci Lett* 317:85–95.
20. Widiyantoro S, van der Hilst R (1996) Structure and evolution of lithospheric slab beneath the Sunda arc, Indonesia. *Science* 271:1566–1570.
21. Teng LS, Lee CT, Tsai YB, Hsiao LY (2000) Slab breakoff as a mechanism for flipping of subduction polarity in Taiwan. *Geology* 28:155–158.
22. Buiter SJH, Wortel MJR, Govers R (1998) The role of subduction in the evolution of the Apennines foreland basin. *Tectonophysics* 296:249–268.
23. Duggen S, Hoernle K, van den Bogaard P, Rüpke L, Morgan JP (2003) Deep roots of the Messinian salinity crisis. *Nature* 422(6932):602–606.
24. Garcia-Castellanos D, Villaseñor A (2011) Messinian salinity crisis regulated by competing tectonics and erosion at the Gibraltar arc. *Nature* 480(7377):359–363.
25. Schott B, Schmeling H (1998) Delamination and detachment of a lithospheric root. *Tectonophysics* 296:225–247.
26. Bercovici D, Ricard Y (2005) Tectonic plate generation and two-phase damage: Void growth versus grain size reduction. *J Geophys Res* 110:B03401.
27. Bercovici D, Ricard Y (2012) Mechanisms for the generation of plate tectonics by two-phase grain-damage and pinning. *Phys Earth Planet Inter* 202-203:27–55.
28. Bercovici D, Ricard Y (2013) Generation of plate tectonics with two-phase grain-damage and pinning: Source–sink model and toroidal flow. *Earth Planet Sci Lett* 365: 275–288.
29. Bercovici D, Ricard Y (2014) Plate tectonics, damage and inheritance. *Nature* 508(7497): 513–516.
30. Ricard Y, Bercovici D (2009) A continuum theory of grain size evolution and damage. *J Geophys Res* 114:B01204.
31. Rozel A, Ricard Y, Bercovici D (2011) A thermodynamically self-consistent damage equation for grain size evolution during dynamic recrystallization. *Geophys J Int* 184:719–728.
32. van Hunen J, van den Berg AP, Vlaar NJ (2002) On the role of subducting oceanic plateaus in the development of shallow flat subduction. *Tectonophysics* 352:317–333.
33. Moresi L, Betts PG, Miller MS, Cayley RA (2014) Dynamics of continental accretion. *Nature* 508(7495):245–248.
34. Bercovici D, Long MD (2014) Slab rollback instability and supercontinent dispersal. *Geophys Res Lett* 41:6659–6666.
35. Riedel MR, Karato S-i (1997) Grain-size evolution in subducted oceanic lithosphere associated with the olivine-spinel transformation and its effects on rheology. *Earth Planet Sci Lett* 148:27–43.
36. Brunet D, Machetel P, Yuen DA (1998) Slab weakening by the exothermic olivine-spinel phase change. *Geophys Res Lett* 25:3231–3234.
37. Newton I (1687) *Philosophiæ Naturalis Principia Mathematica* (Edmund Halley, London).
38. Ricard Y, Froidevaux C (1986) Stretching instabilities and lithospheric boudinage. *J Geophys Res* 91:8314–8324.
39. Ricard Y (1986) Dynamique interne de la Terre et observations gravimétriques. PhD thesis (University Paris XI, Orsay, France).
40. Smith CS (1948) Grains, phases, and interfaces: An interpretation of microstructure. *Trans AIME* 175:15–51.
41. Wörner C, Cabo A (1987) On the grain growth inhibition by second phases particles. *Acta Metall* 35:2801–2804.
42. Evans B, Renner J, Hirth G (2001) A few remarks on the kinetics of static grain growth in rocks. *Int J Earth Sci* 90:88–103.